Simulation of an atomistic dynamic field theory for monatomic liquids: Freezing and glass formation

Joel Berry,[1] K. R. Elder,[2] and Martin Grant[1]
[1]*Physics Department, McGill University, Rutherford Building, 3600 rue University, Montréal, Québec, Canada H3A 2T8*
[2]*Department of Physics, Oakland University, Rochester, Michigan 48309-4487, USA*
(Received 19 July 2007; revised manuscript received 30 March 2008; published 9 June 2008)

We examine a phase field crystal model for simple liquid-solid systems consisting of a free energy functional related to the Ramakrishnan-Yussouff free energy of classical density functional theory and an equation of motion capable of describing long-time-scale behavior in the deeply supercooled regime. The thermodynamics and dynamics of freezing and glass formation in this model system are studied through large-scale three-dimensional Langevin simulations. At low cooling rates bcc crystals are formed by nucleation and growth from the melt. At large cooling rates no clear glass transition is observed, but a kinetically driven first-order transition from supercooled liquid to a disordered glasslike solid does occur. Despite the peculiarities of the transition, the structure and properties of the resulting disordered solid are shown to strongly resemble those of a typical glass. Consequences of pseudocritical behavior and heterogeneity near the liquid spinodal are also discussed.

DOI: 10.1103/PhysRevE.77.061506 PACS number(s): 64.70.P−, 64.70.D−, 61.43.−j, 81.05.Kf

When a simple liquid is supercooled below its freezing temperature, a crystalline solid typically becomes the state of lowest free energy and a first-order crystallization transition may occur. If the liquid is supercooled very rapidly, crystallization may be avoided, with the liquid instead undergoing a characteristic rapid but continuous slowing accompanied by very little structural change—a glass transition. Much of the phenomenology of the glass transition has long been firmly established, but a comprehensive understanding of the underlying mechanisms giving rise to glass formation has not been realized. Some success has been achieved with approaches such as mode coupling theory and molecular dynamics simulations in understanding important aspects of the dynamics of moderately supercooled liquids. Such descriptions are generally limited to time scales roughly ten orders of magnitude shorter than those near the laboratory glass transition temperature T_g and therefore to the initial stages of the glass-formation process.

In this paper we examine a model for simple liquids that is capable of accessing the rapidly slowing dynamical region near T_g. Our approach is related to the classical density functional theory of freezing [1,2] and to the variously proposed dynamical extensions of density functional theory [3–9]. The utility of dynamic density approaches in modeling the glass transition lies in their combination of coarse-grained free energies with mesoscopic equations of motion, which together provide a thermodynamic description of atomic structure and dynamics over long time scales.

Most density functional studies of glass formation have focused on the static properties of the free energy functional, using various analytic or numerical approximations to locate and characterize metastable minima with aperiodic or glasslike density structures at large supercoolings [10–16]. Early dynamical simulations of the weakly inhomogeneous supercooled liquid have been performed using nonlinear fluctuating hydrodynamics [17]. Despite the insights gained from these approaches, results involving dynamics have been limited and there remains a need for considerable advancement in terms of finding less restricted solutions, studying larger systems, and thoroughly examining dynamic behavior in both the ergodic and nonergodic regimes. We report here on initial work toward these objectives.

The phase field crystal (PFC) method [18], like dynamic density functional theories, consists of a free energy which is a functional of the microscopic time-averaged atomic number density and an equation of motion obeying Langevin dynamics. The specific forms of the free energy and equation of motion allow us to conduct numerical simulations which access system sizes several orders of magnitude larger than previous density functional studies and simulation times on the order of 10^4-10^6 typical liquid relaxation times. This corresponds to time scales several orders of magnitude longer than those accessible to typical molecular dynamics simulations. The glasslike metastable states are obtained in a physically meaningful way with no explicit restrictions on the solution set. The packing structure and local density profiles are naturally optimized and are found to exhibit heterogeneity in local mean square displacements. A related methodology has recently been proposed and applied to the creation of amorphous structures in two dimensions without thermal noise [19].

As shown previously [20], the form of the PFC free energy can be derived directly from the Ramakrishnan-Yussouff free energy of density functional theory [21]. Here we are initially interested in single-component systems, though the approach is straightforwardly generalized to systems with arbitrarily many components. The postulated Helmholtz potential of a single-component system is given by

$$\frac{\mathcal{F}}{k_B T} = \int d\vec{r}[\rho(\vec{r})\ln(\rho(\vec{r})/\rho_\ell) - \delta\rho(\vec{r})] - \frac{1}{2}\int d\vec{r}\, d\vec{r}'\, \delta\rho(\vec{r}) C_2(\vec{r},\vec{r}')\, \delta\rho(\vec{r}') + \cdots, \qquad (1)$$

where $\rho(\vec{r})$ is the number density, ρ_ℓ is the density of a ref-

erence liquid state, $\delta\rho(\vec{r}) \equiv \rho(\vec{r}) - \rho_\ell$, and $C_2(\vec{r},\vec{r}')$ is the two-point direct correlation function of the reference liquid state. To generate a PFC free energy, Eq. (1) is truncated at C_2 and expanded around the rescaled density $n \equiv (\rho - \bar{\rho})/\bar{\rho}$ up to n^4, where $\bar{\rho}$ is the average number density. It is furthermore assumed that C_2 can be represented by its expansion in a Fourier series,

$$\hat{C}_2(k) = \hat{A}_0 + \hat{A}_2 k^2 + \hat{A}_4 k^4 + \cdots, \tag{2}$$

where $\hat{A}_0$, $\hat{A}_2$, and $\hat{A}_4$ are negative, positive, and negative, respectively. The simplest physically meaningful form for $\hat{C}_2(k)$ is generated by truncating the series at k^4, and the final result is a PFC free energy,

$$F = \int d\vec{r}\left(\frac{B^\ell}{2}n^2 + \frac{B^s}{2}n(2\nabla^2 + \nabla^4)n - v\frac{n^3}{6} + \frac{n^4}{12}\right), \tag{3}$$

where $F \equiv (\mathcal{F} - \mathcal{F}_0)/(\bar{\rho}k_B T R^d)$, $\mathcal{F}_0$ is the free energy functional at constant density, $B^\ell \equiv 1 - \bar{\rho}\hat{A}_0$, $B^s \equiv \bar{\rho}\hat{A}_2^2/4|\hat{A}_4|$, $R \equiv \sqrt{2|\hat{A}_4|/\hat{A}_2}$, and v accounts for the lowest-order contribution from C_3.

The PFC free energy therefore corresponds to a specific parametrization of the full density functional form, where the logarithmic term has also been approximated by a truncated expansion in n. As we will demonstrate, this simplified form exhibits the same qualitative behavior in terms of freezing and glass formation as Eq. (1), but is considerably simpler to manipulate and simulate numerically. A consequence of the approximations used may be a restriction on the number of systems and the range of conditions which can be quantitatively described.

The appropriate dynamics for a glass-forming liquid described by a mesoscopic free energy has been debated among practitioners of the various forms of dynamic density functional theory and other related field theories. We choose in this initial study to focus primarily on the simplest form potentially capable of capturing the relevant behavior,

$$\frac{\partial n}{\partial \tau} = \nabla^2 \frac{\delta F}{\delta n} + \eta, \tag{4}$$

where $\tau \equiv \Gamma k_B T R^{d-2} t$ is the dimensionless time (referred to hereafter as t), η is a Gaussian stochastic noise term with $\langle \eta(\vec{r}_1,t_1)\eta(\vec{r}_2,t_2)\rangle = D\nabla^2\delta(\vec{r}_1 - \vec{r}_2)\delta(t_1 - t_2)$, and in this study $D \equiv 3/[\alpha(\bar{\rho}R^d)^2]$. α is used to vary the relative magnitude of the thermal fluctuations to the free energy topology. This equation describes a conserved density field $n(\vec{r})$ undergoing a purely diffusive free energy minimization in the presence of random thermal fluctuations.

The most common dynamic density functional equation of motion also maintains density conservation and roughly diffusive free energy minimization, but introduces a local density-dependent mobility and multiplicative thermal noise. With the rescaled density n, it has the form

$$\frac{\partial n}{\partial \tau} = \vec{\nabla}\cdot\left((n+1)\vec{\nabla}\frac{\delta F}{\delta n}\right) + \nu, \tag{5}$$

where $\langle \nu(\vec{r}_1,t_1)\nu(\vec{r}_2,t_2)\rangle = D\vec{\nabla}\cdot\vec{\nabla}[(n+1)\delta(\vec{r}_1 - \vec{r}_2)\delta(t_1 - t_2)]$. Though these effects may play a role in glass formation, we will report only results obtained using Eq. (4) and note that initial simulations of Eq. (5) show qualitatively similar results. For a small-n expansion, if $n \ll 1$, we have $n+1 \simeq 1$ and Eq. (5) reduces to Eq. (4), including the noise term. For highly inhomogeneous states the differences may become significant. A more detailed comparison of the two forms will be given in a future presentation.

A semi-implicit pseudospectral algorithm was used to solve Eq. (4) in three dimensions with periodic boundary conditions (see the Appendix for details). The parameters used were $\Delta x = 1$, $\Delta\tau = 0.5$, $B^s = \sqrt{3}/3$, and $v = 3^{1/4}/2$, while system sizes were varied from $V = 64^3$ to 512^3 ($\sim$686 to $\sim$390 224 atoms). Sizes of $V \gtrsim 128^3 - 256^3$ are required to overcome finite-size effects discussed in Sec. III.

I. FREEZING TRANSITION

At high temperatures the equilibrium phase for the time-averaged number density $n(\vec{r})$ is a spatially uniform fluid state. For off-critical average densities, as the dimensionless temperature parameter $T \equiv B^\ell - B^s$ is lowered, the liquid passes through a first-order phase transition point below which the equilibrium phase is one with periodic density modulations, corresponding to a bcc crystalline state. Due to the nucleation barrier between the liquid and solid phases, the liquid can be supercooled until the spinodal temperature T_s is approached and the free energy barrier eventually vanishes.

A. Coexistence region (nonspinodal)

Previous density functional studies [10–15] and others [19,22] find that, for sufficiently large supercooling, a large number of metastable states with aperiodic density modulations and with $F_{\text{cryst}} < F < F_{\text{liquid}}$ become accessible by a first-order transition. Our simulations show that this discontinuous transition to a glasslike state does occur and also demonstrate that the structure of the resulting solid phase depends primarily on the cooling rate $\dot{T}$. Very low cooling rates lead to bcc structures, generally through a two-stage nucleation process involving an initial disordered solid which quickly rearranges into a bcc crystal. As $\dot{T}$ is increased, the stability of the initial disordered solid grows and it persists for longer and longer times. Finally, at cooling rates above the critical cooling rate $\dot{T}_c$, the amorphous solid is relatively stable for times longer than the time scale of the simulations. Here the system is kinetically limited and becomes trapped in the metastable disordered state, unable to organize with the symmetry of lowest free energy.

This cooling rate effect is illustrated in Fig. 1, where two examples of the free energy change with temperature are shown, one for high and one for low $\dot{T}$. Sample configurations obtained at various cooling rates are also shown in Fig.

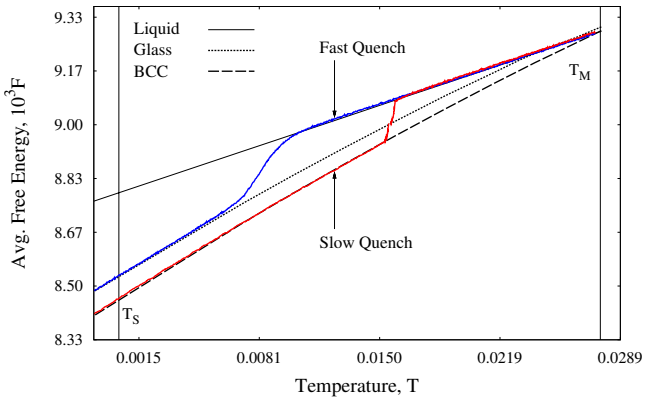

FIG. 1. (Color online) Free energies of various phases vs T. Disordered solid F is representative result from a single rapid quench, as F varies significantly only for $\dot{T}$ near $\dot{T}_c$. Example fast and slow quenches are overlaid to illustrate the effect of cooling rate.

2, where the gradual shift toward bcc order is evident. There appears to be no Kauzmann temperature at which the entropies $(S=-\partial F/\partial T)$ of the amorphous and bcc phases would cross [23].

Since the disordered solid forms through a nucleation process, classical nucleation theory can be used to analyze the transition behavior near the liquid-bcc coexistence region. Critical radii R_c have been measured for bcc and disordered solid droplets in liquid at various temperatures, as shown in Fig. 3. The two structures are found to have essentially equivalent R_c, except near the equilibrium bcc melting temperature T_m, where the disordered solid phase is increasingly unstable and tends to crystallize in very short times. For small R_c, the critical radii are discretized to values corresponding approximately to atomic neighbor distances, while the larger R_c diverge more smoothly, following $R_c \propto (T_m - T)^{-1}$ as predicted by classical nucleation theory. The results indicate that the free energy barrier between liquid and disordered solid is consistently 10–25 % smaller than the barrier between liquid and bcc (Fig. 3 inset). The predicted nucleation times $t_n \propto e^{\Delta F/k_B T}$ are at least one order of magnitude smaller for the disordered solid than for the bcc structure, explaining the initial presence of disordered droplets in all quenching simulations.

B. Spinodal effects

The preceding discussion of freezing applies to the general case in which the first-order liquid to disordered solid transition occurs at low to moderate supercooling (weak-coupling regime, $0<\alpha\lesssim 0.1$). When the liquid can be supercooled very deeply, near its spinodal temperature T_s, pseudocritical effects emerge with the underlying continuous transition. Similarities between the near-spinodal liquid and glass-forming liquids have been examined by other authors [22,24,25]. Here we find that, despite the appearance of the onset of glass-formation near T_s—signaled by a diverging relaxation time, stretched exponential decay, and spatial heterogeneity in local relaxations—the pseudocritical effects play only a secondary role in the freezing process. They have little bearing on whether the resulting solid is disordered or crystalline, and therefore do not appear to be associated with a true glass transition in this system, as discussed in the following.

The density autocorrelation relaxation function $S(k,t) = \langle \hat{n}(k,t)\hat{n}(k,0)\rangle$ for the liquid can be calculated at the linear level by solving the equation of motion for the linearized chemical potential $(\delta F/\delta n)$ in Fourier space, giving

$$S(k,t) \simeq e^{-t/\tau} S(k,0) \tag{6}$$

where $\tau=[2k^2(T+B^s-2B^sk^2+B^sk^4)]^{-1}$ is the density autocorrelation relaxation time. This solution for τ is plotted in Fig. 4 along with measurements from numerical simulations. Without fluctuations, τ diverges at $T_s=0$ for $k=1$. The often used Vogel-Fulcher fit,

$$\tau = A e^{B/(T-T_s)}, \tag{7}$$

where A and B are constants, is reasonably accurate very near T_s, but our analysis clearly points to a power law divergence of the form $\tau \sim (T-T_s)^{-1}$.

Measurements of $S(k,t)$ also indicate that the PFC liquid exhibits increasingly stretched exponential decay as T_s is approached. Fits to the form

$$S(k,t) = e^{-(t/\tau)^\beta} \tag{8}$$

indicate that the stretching exponent β decreases from near 1 to approximately 0.75 near T_s (Fig. 4 inset). This apparent stretching coincides with, and is in part caused by, the onset of increasing dynamic heterogeneity near the liquid spinodal. Well above T_s, the local relaxation times τ_ℓ are fairly homogeneous across all regions of the liquid. Near T_s the width of the τ_ℓ distributions increases dramatically (along with the average relaxation time), approximately following a $(T-T_s)^{-1}$ divergence. This signifies growing heterogeneity, as different regions in the system are relaxing with a larger and larger disparity of rates. Spatial correlations of local relaxation times will require further examination to discuss conclusively, but we note that the most mobile regions tend to be arranged in stringlike clusters which surround the less mobile regions.

The preceding pseudocritical behaviors appear to indicate that the supercooled liquid near T_s is undergoing a continuous transition to an effectively frozen state, somewhat resembling the behavior of a fragile glass former. We find that thermal fluctuations eventually truncate this pseudocritical behavior and near T_s the initially continuous slowing of dynamics is overridden by the first-order freezing transition. Therefore, even when spinodal effects are strong the transition from liquid to disordered solid is ultimately first order in this system, and the suggestive pseudocritical behavior has relatively little bearing on whether the resulting solid is glasslike or crystalline. Global instability to nucleation for $T\lesssim T_s$ seems to be one way in which a near-spinodal liquid differs from a glass-forming liquid, which by contrast remains robust to first-order discontinuities at all temperatures (for sufficiently rapid quench).

The appearance of an amorphous solid rather than a crystalline solid upon quenching *below the spinodal* in two di-

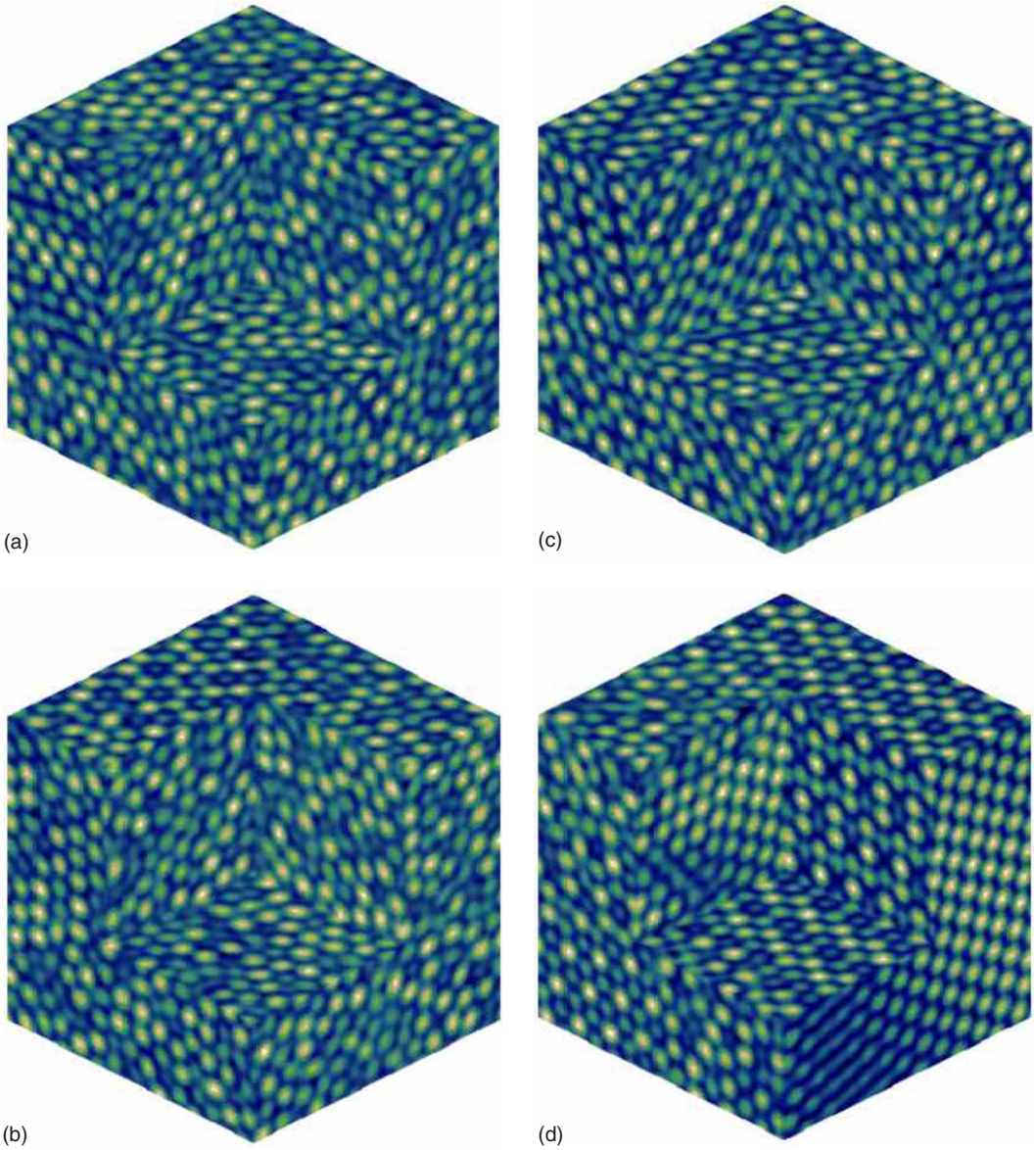

FIG. 2. (Color online) Sections of $n(\vec{r})$ from systems quenched at various cooling rates. Light areas correspond to high density, dark areas to low density. $T_{\text{init}}=0.0020$, $T_{\text{final}}=-0.0014$, and $V=256^3$. Each cube shown contains a region $V=96^3$, or ~5% of its system's overall volume. (a) $1.3\times10^{-7}T/t$, (b) $6.4\times10^{-8}T/t$, (c) $2.6\times10^{-8}T/t$, (d) $6.4\times10^{-9}T/t$.

mensions has been discussed in a similar context [19]. Deep quenches below T_s were shown to generate instability across a broad range of wave vectors, preventing the growing droplets from selecting a single wave vector corresponding to the ordered structure. This picture is consistent with simulation results for subspinodal quenches presented here, and we find additionally that sufficiently slow quenches facilitate formation of the equilibrium crystal structure, regardless of proximity to T_s.

II. DISORDERED PHASE STRUCTURE AND PROPERTIES

The structure of the PFC disordered solid phase is consistent with that of many known glass formers, having a structure factor $S_p(k)$ and radial distribution function $g_p(R)$ that are liquidlike and exhibit the characteristic split second peak. $S_p(k)$ and $g_p(R)$ are the spherically averaged structure factor and radial distribution function, respectively, of the most probable atomic configuration. Examples of $S_p(k)$ are shown in Fig. 5 for various cooling rates $\dot{T}$. The disordered structures obtained at large $\dot{T}$ are qualitatively similar to but quantitatively different from the Bernal packing scheme. As $\dot{T}$ is decreased the structure factor of the resulting solid develops more prominent peaks all corresponding to diffraction peaks in a bcc crystal (see Fig. 5 inset), and visual inspection reveals that sizable regions with bcc order have formed, as is clearly seen in Fig. 2.

Analysis of local, short-range order was performed on many amorphous configurations, and representative data for the average coordination number z as a function of coordination sphere radius R_{CN} is shown in Fig. 6. The bcc result

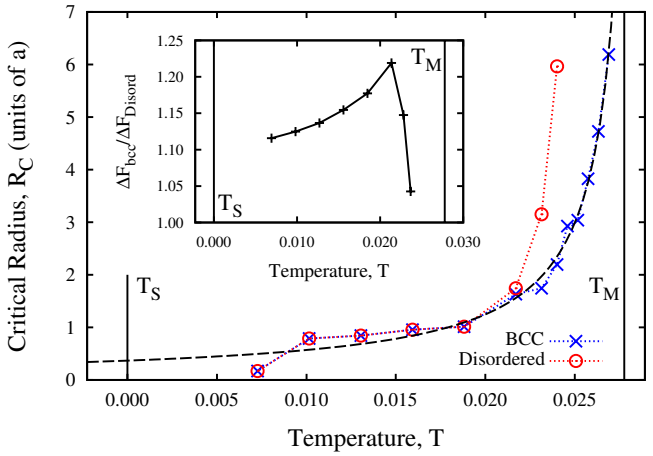

FIG. 3. (Color online) Measured critical radii of disordered solid and bcc phases in liquid at various T, in units of the equilibrium one-mode bcc lattice constant a. The dashed line is a fit to classical nucleation theory where $R_c \propto (T_m - T)^{-1}$. Inset: Calculated ratio of bcc to disordered solid free energy barriers from classical nucleation theory.

exhibits clear steps at values of $z=8,14,26,\ldots$, as can be readily calculated. The disordered solid result shows a much more gradual rise in z, to a near plateau at $z \simeq 13$, and then further increase. A histogram of coordination numbers at $R_{CN}=1.18a_{bcc}$ is shown in the inset of Fig. 6. These results compare favorably with values for various binary metallic glasses obtained using *ab initio* molecular dynamics [26].

We can also define an effective packing fraction σ as

$$\sigma = \frac{N}{N_{bcc}} \sigma_{bcc}, \tag{9}$$

where N is the number of density peaks in the system, N_{bcc} is the number that would be found in an ideal bcc system of the same size, and $\sigma_{bcc}=0.68$ is the ideal bcc packing fraction. Measurements indicate that $\sigma \simeq 0.63-0.64$, with 0.64 being the apparent limiting value for the disordered phase. This is compared to $\sigma=0.61$ for the Bennett hard-sphere glass [27] and $\sigma=0.6366$ for dense randomly packed ball bearings [28]. Thus, in many respects, the structure of the disordered solid phase is consistent with that of simple structural glasses as observed experimentally and in atomistic computer simulations.

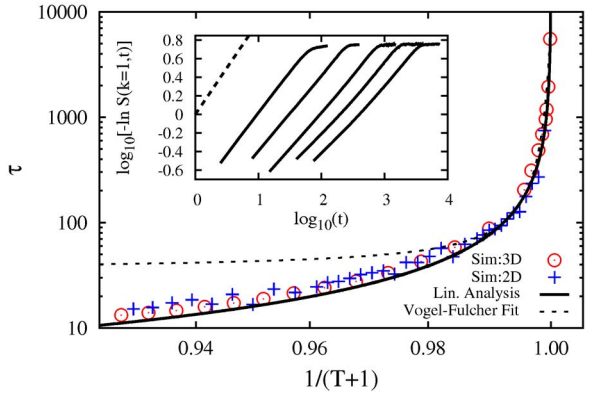

FIG. 4. (Color online) Divergence of the density autocorrelation relaxation time for two- and three-dimensional systems (τ_{2D} scaled). Relaxation data taken near the first peak in $S(k)$ at $k=1$. Additional orders of magnitude in time can be simulated, but here nucleation occurs rapidly for T very near T_s, making the T axis the limiting factor. Inset: Stretching relaxation functions as T decreases from left to right. The dashed line corresponds to normal exponential decay ($\beta=1$).

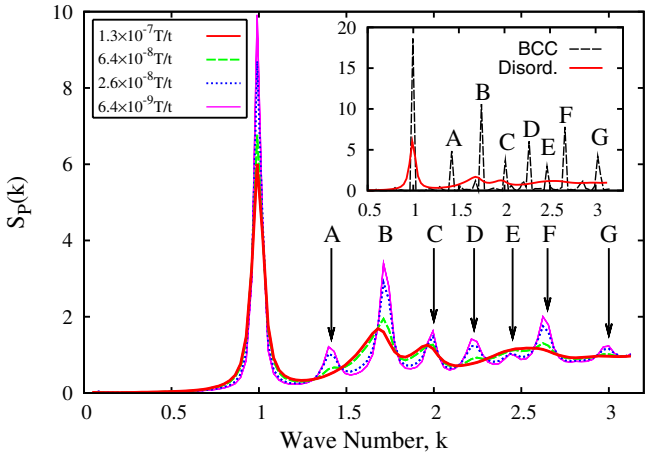

FIG. 5. (Color online) Most probable instantaneous solid structure factors $S_p(k)$ at various cooling rates. Data for systems shown in part in Fig. 2. Wave numbers corresponding to bcc peaks are labeled with letters. Inset: bcc and disordered solid $S_p(k)$.

As noted, the PFC disordered solid also exhibits spatial heterogeneity in local mean square displacements (MSDs), with a distribution of local MSDs several times broader than that of the bcc phase (Fig. 7 inset). The variance of this distribution, as shown in Fig. 7, is found to diverge approximately as $(T_m - T)^{-1}$ as the disordered solid is heated, while the bcc phase shows a much weaker increase in heterogeneity before melting. This behavior is related to the phenom-

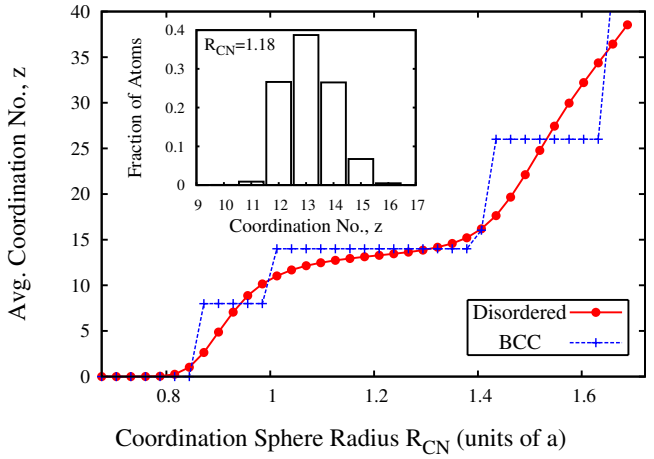

FIG. 6. (Color online) Coordination number vs coordination sphere radius for most probable atomic structures of representative disordered and bcc systems, in units of the equilibrium one-mode bcc lattice constant a. Inset: Histogram of coordination numbers at $R_{CN}=1.18$.

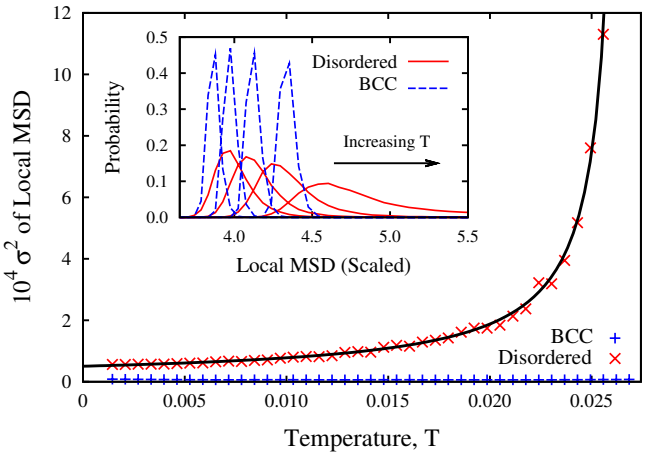

FIG. 7. (Color online) Variance in the distribution of local MSDs in disordered and bcc samples vs temperature. The solid line is a power law fit with exponent −1. Inset: Local MSD distributions at various temperatures.

enon of critical softening in glasses, where the relative solidity of a glass, as measured by the Debye-Waller factor, decreases with strong nonlinearity at high temperatures [29].

III. SYSTEM SIZE AND AGING

For relatively small systems ($V \lesssim 128^3$–256^3) the gradual sequence of structures leading from the maximally disordered state to the perfect bcc state becomes increasingly restricted. Only highly disordered or highly ordered states are generally observed below this range. Such a restriction on the possible states has significant effects on the relaxation of the disordered solid toward the lower-energy crystalline state. Very little aging of a disordered system is possible when the intermediate phases of mixed character are inaccessible, and the disordered solid is effectively frozen in or near its initial minima for times longer than the simulations. In sufficiently large systems, a more systematic aging behavior is observed. Thermal fluctuations lead to small local rearrangements in $n(\vec{r})$, sometimes cascades of rearrangements, which lower F incrementally toward that of the bcc state. The rate of relaxation is strongly dependent on $\dot{T}$.

Therefore, even though the structural correlation lengths in a glasslike system are expected to be only on the order of a few atomic spacings, we find that the system size must be considerably larger to avoid finite-size effects in the relaxational dynamics of the nonequilibrium state. In comparison, the more homogeneous supercooled liquid phase exhibits finite-size effects only near T_s, where the correlation length becomes large.

IV. DISCUSSION AND CONCLUSIONS

We have demonstrated by direct numerical simulation and analysis that the monatomic PFC model exhibits a range of freezing behaviors which depend primarily on the quench rate and proximity to the liquid spinodal temperature. When freezing occurs well above T_s, the transition is strongly first order and in qualitative agreement with classical nucleation theory. Simulations indicate that the initial nucleites are relatively disordered with high probability, regardless of the cooling rate. As the nucleites grow and coalesce, they either remain disordered and glasslike if the quench is sufficiently rapid, or rearrange locally into the equilibrium bcc structure if the quench is slow. Thus glass formation in this regime is kinetically driven but strongly first order, with no accompanying continuous slowing of liquid dynamics as is characteristic of a typical glass former.

When freezing occurs near T_s, the supercooled liquid does exhibit pseudocritical behaviors which somewhat resemble the onset of a glass transition. These include a diverging relaxation time, stretched exponential decay, and apparent dynamic heterogeneity. We believe that these are not associated with a true glass transition in this system, as the kinetically driven first-order transition ultimately intervenes near T_s, and the preceding pseudocritical effects serve only to alter the critical cooling rate and not the qualitative nature of glass formation as described above.

Despite the fact that formation of the disordered solid phase stems from a kinetically driven first-order transition rather than a clear glass transition, the structure and properties of the disordered solid appear to be consistent with those of simple glasses. The monatomic PFC free energy clearly contains inherent glasslike minima but accesses them by a dynamic pathway that does not resemble a glass transition. This could be a peculiarity of simple monatomic systems, which have not been shown to undergo a glass transition experimentally, presumably due to cooling rate limitations, and have received only limited attention in atomistic simulations, though available results seem to indicate that initial signs of a glass transition may be observed on short time scales and are typically followed by rapid crystallization. Alternatively, it is possible that such systems should exhibit a clear glass transition at very large cooling rates, and the coarse-grained PFC model does not adequately capture all important aspects of the glass-forming dynamics, such as those on shorter time scales or those generated by an equation of motion such as Eq. (5). If a suitable size and/or mobility difference between species is fundamental to glass formation, or at least strongly enhances glass formability, then the lack of a clear glass transition here would not be surprising. Clarification should come from our study of binary systems currently under way, where the role of size and mobility differences can be considered, and the liquid-to-glass transition is clear and well documented.

ACKNOWLEDGMENTS

J.B. acknowledges support from the Richard H. Tomlinson and Carl Reinhardt Foundations. K.R.E. would like to acknowledge support from the National Science Foundation under Grant No. DMR-0413062. M.G. acknowledges the National Science and Engineering Research Council of Canada and le Fonds Quebecois de la Recherche sur la Nature et les Technologies for support.

APPENDIX: NUMERICAL METHOD

A semi-implicit, pseudospectral numerical method was used to simulate the PFC dynamics. A similar method has

been reported in [30]. In three dimensions, this algorithm results in one to two orders of magnitude improvement in computational efficiency compared to the familiar real space finite-difference Euler scheme. The noiseless algorithm is written in Fourier space as

$$\hat{n}_{t+1} = \frac{\hat{n}_t - k^2 \Delta t[(1/3)\hat{n}_t^3 - (\nu/2)\hat{n}_t^2]}{1 + k^2 \Delta t(B^\ell - 2B^s k^2 + B^s k^4)},$$

where $\hat{n}_t$ is the Fourier transform of $n(\vec{r})$ at time step t, k is the Fourier mode, and Δt is the time step. A Gaussian stochastic noise term η is applied to the updated density field at each time step. It is calculated by producing three independent Gaussian random numbers ν at each grid point (i,j,k) such that

$$\eta_{ijk} = \frac{\nu^{(1)}_{i+1,j,k} - \nu^{(1)}_{i,j,k} + \nu^{(2)}_{i,j+1,k} - \nu^{(2)}_{i,j,k} + \nu^{(3)}_{i,j,k+1} - \nu^{(3)}_{i,j,k}}{\Delta x}$$

where

$$\langle \nu^{(a)}_{i,j,k}(p) \nu^{(b)}_{l,m,n}(q) \rangle = \frac{D\Delta t}{(\Delta x)^d} \delta_{i,l} \delta_{j,m} \delta_{k,n} \delta_{p,q} \delta_{a,b}.$$

[1] Y. Singh, Phys. Rep. **207**, 351 (1991).
[2] D. Oxtoby, Annu. Rev. Mater. Res. **32**, 39 (2002).
[3] B. Kim and K. Kawasaki, J. Phys. A **40**, F33 (2007).
[4] A. Andreanov, G. Biroli, and A. Lefévre, J. Stat. Mech. (2006) P07008.
[5] D. Dean, J. Phys. A **29**, L613 (1996).
[6] K. Fuchizaki and K. Kawasaki, J. Phys.: Condens. Matter **14**, 12203 (2002).
[7] U. Marconi and P. Tarazona, J. Chem. Phys. **110**, 8032 (1999).
[8] A. Perez-Madrid, D. Reguera, and J. Rubi, J. Phys.: Condens. Matter **14**, 1651 (2002).
[9] T. Munakata, Phys. Rev. E **67**, 022101 (2003).
[10] Y. Singh, J. P. Stoessel, and P. G. Wolynes, Phys. Rev. Lett. **54**, 1059 (1985).
[11] C. Dasgupta and S. Ramaswamy, Physica A **186**, 314 (1992).
[12] C. Kaur and S. P. Das, Phys. Rev. Lett. **86**, 2062 (2001).
[13] K. Kim and T. Munakata, Phys. Rev. E **68**, 021502 (2003).
[14] S. P. Singh and S. P. Das, J. Phys.: Condens. Matter **19**, 246107 (2007).
[15] T. R. Kirkpatrick and P. G. Wolynes, Phys. Rev. A **35**, 3072 (1987).
[16] C. Dasgupta and O. T. Valls, Phys. Rev. E **59**, 3123 (1999).
[17] L. M. Lust, O. T. Valls, and C. Dasgupta, Phys. Rev. E **48**, 1787 (1993).
[18] K. R. Elder and M. Grant, Phys. Rev. E **70**, 051605 (2004).
[19] Y. M. Jin and A. G. Khachaturyan, J. Appl. Phys. **100**, 013519 (2006).
[20] K. R. Elder, N. Provatas, J. Berry, P. Stefanovic, and M. Grant, Phys. Rev. B **75**, 064107 (2007).
[21] T. V. Ramakrishnan and M. Yussouff, Phys. Rev. B **19**, 2775 (1979).
[22] W. Klein, H. Gould, R. A. Ramos, I. Clejan, and A. I. Mel'cuk, Physica A **205**, 738 (1994).
[23] Extrapolation of the data above T_s does predict a crossover, but as additional data below T_s are included, S_{disord} is found to approach but not cross S_{bcc}.
[24] G. Johnson, A. I. Mel'cuk, H. Gould, W. Klein, and R. D. Mountain, Phys. Rev. E **57**, 5707 (1998).
[25] W. Klein, H. Gould, J. Tobochnik, F. J. Alexander, M. Anghel, and G. Johnson, Phys. Rev. Lett. **85**, 1270 (2000).
[26] H. Sheng, W. Luo, F. Alamgir, J. Bai, and E. Ma, Nature (London) **439**, 419 (2006).
[27] C. Bennett, J. Appl. Phys. **43**, 2727 (1972).
[28] J. Finney, Proc. R. Soc. London, Ser. A **319**, 479 (1970).
[29] W. Gotze, in *Liquids, Freezing and Glass Transition*, edited by J. Hansen, D. Levesque, and J. Zinn-Justin (North-Holland, Amsterdam, 1991).
[30] M. Cheng and J. Warren, e-print arXiv:physics/0611243.